The Kármán Vortex Street—
LDV and PIV Measurements Compared with CFD

Oliver Pust and Christoph Lund

Department of Fluid Mechanics, Faculty of Mechanical Engineering
University of the Federal Armed Forces Hamburg, D–22039 Hamburg, Germany

1 Introduction

The laminar flow of an incompressible newtonian fluid around a circular cylinder is well known and described in literature as *Kármán vortex street*. For its extensive investigations in the past this flow is frequently used as a test case for numerical simulation (CFD). In spite of that, direct comparisons of the time dependent development of the velocity components between experiment and simulation still seem to be missing. Until now to our knowledge just comparisons for the mean values have been reported. In this work results for the time dependent flow obtained with Laser Doppler Velocimetry (LDV) and Particle Image Velocimetry (PIV) are reported and compared to results of a numerical simulation. The qualitative and quantitative correspondences and differences are presented and discussed.

2 Experimental set-up

Figure 1 shows the side view and the partial top view of the set-up. The dotted area comprising the cylinder and its wake—where vortex shedding is expected—represents the region of interest both for experiment and numerical simulation. Details are shown in figure 2 with (ξ, ψ) defining a dimensionless coordinate system in which the cylinder diameter is used as a reference length. The region of interest is 352 mm in length, 65.6 mm in height and 328 mm in depth. The cylinder has a diameter of 16 mm and extents over the whole channel depth with 328 mm in length. The measurements are conducted at half channel depth where the flow is taken to be two-dimensional[1]. At the beginning of the channel a honeycomb flow guide is installed in order to reduce inflow effects that are caused by the 90° change in direction of the flow from the reservoir to the channel.

The fluid (water) is pumped into the reservoir by a centrifugal pump. The flow rate is adjusted to its desired value by an electronically controllable valve and measured simultaneously. Behind the valve the water is stored in an open tank from which it is pumped back into the reservoir. So we have a circular flow that allows us to seed the fluid only once before the measurements start. At all times we pump more water into the reservoir than is needed for the desired maximum flow rate. The unused water flows back into the tank via a wasteway. So the water level in the

[1]The geometrical ratios of this two-dimensional problem are taken from [3].

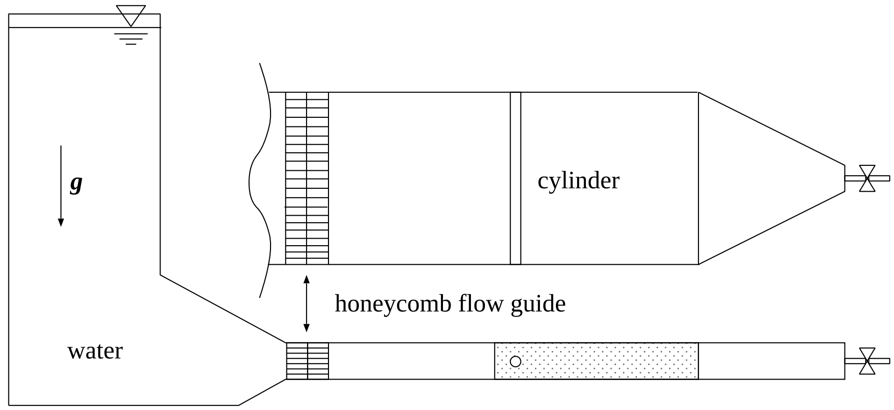

Fig. 1. Sketch of the set-up (side view and partial top view)

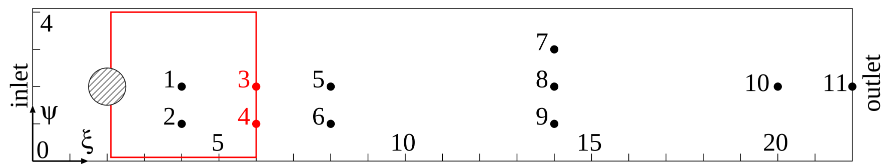

Fig. 2. Geometry of the channel and location of the measuring points

reservoir is kept constant, thus ensuring an also constant pressure gradient along the channel.

For the LDV measurements a two component backward scattering system (DANTEC) with an Argon-Ion-Laser is used. The measuring volume (0.2 mm $\times$ 0.2 mm $\times$ 2 mm) is traversed within a plane in the middle of the channel that is orientated normally to the cylinder axis. The location of the measuring points can be seen in figure 2. The tracers used are titanium-oxid particles with a mean diameter of 5 µm.

For the PIV measurements a system (Optical Flow Systems Ltd.) is used that mainly consists of a double oscillator Nd:YAG laser (30 mJ per cavity), a cross-correlation CCD-camera with a 1 K by 1 K sensor and a PC equipped with 512 MB RAM in order to record sufficiently long time series of the flow. The area recorded by the CCD-camera is described by a square with its lower left corner at $(\xi = 2.1, \psi = 0.1)$ and its upper right corner at $(\xi = 6.0, \psi = 4.0)$. For better light scattering efficiency the tracers used are silver-coated hollow glass-spheres with a mean diameter of 10 µm.

We define a Reynolds number that characterizes the stationary flow in the middle plane as

$$\mathrm{Re} = \frac{u_\mathrm{m} D \rho}{\mu} \tag{1}$$

with the average horizontal velocity u_m, the newtonian dynamic viscosity μ, the fluid density ρ and the cylinder diameter D. The value of u_m is determined by integrating the inflow velocity profile ($\xi = -2$) (see figure 3(a)) over the channel height thus giving a Reynolds number of 100.

Further the Strouhal number Sr and the dimensionless time $\tilde{t}$

$$\mathrm{Sr} = \frac{D f}{u_{\mathrm{m}}} \quad , \quad \tilde{t} = \frac{t\,\mu}{\rho D^2} \tag{2}$$

with the separation frequency f of the vortices are used. Thus the dimensionless time is calculated to $\tilde{t} = t/256$ s. All velocities are made dimensionless with u_{m}.

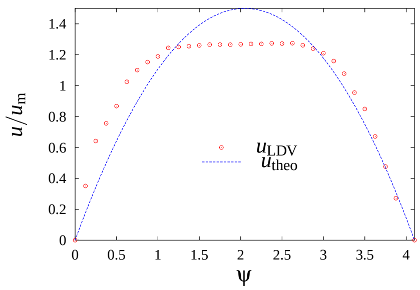

(a) Horizontal component

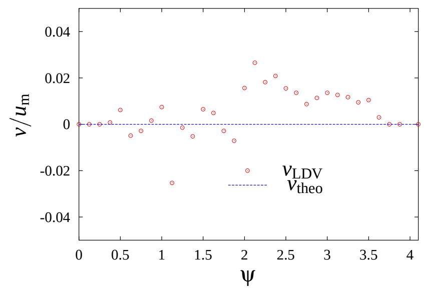

(b) Vertical component

Fig. 3. Inflow velocity profile at $\xi = -2$

In the stationary case the inflow should ideally be fully developed, time independent and of parabolic shape across the channel height. As one can see in figure 3 the inflow is not of parabolic shape and shows a small vertical component ($\approx 2\%$ of u_{m}). The reason for the non-parabolic shape obviously is that the length of the inlet is too short to allow the flow to fully develop. The vertical component that results from the 90° change in direction of the flow from the reservoir to the channel is limited to an acceptable value by the already mentioned flow guide at the beginning of the inlet. Nevertheless this inflow profile is used for the numerical simulation so that direct comparison is possible.

3 Numerical Simulation

The primary aim of the simulation is to compute the velocity in the mid-plane area shown in figure 2, where the flow is assumed to be two-dimensional. Using a primitive-variable formulation with cartesian velocity $\mathbf{v}(u,v)$ and pressure p, the simulation is based on the equation of motion for an incompressible isothermal fluid

$$\rho \left(\frac{\partial \mathbf{v}}{\partial t} + \mathbf{L} \cdot \mathbf{v} \right) = -\mathrm{grad}\, p + \mathrm{div}\, \mathbf{T} + \mathbf{f} \tag{3}$$

and the continuity equation

$$\operatorname{div} \mathbf{v} \;=\; 0. \tag{4}$$

Here t represents the time, ρ the fluid density, $\mathbf{L}$ the velocity gradient ($\mathbf{L} = \operatorname{grad} \mathbf{v}$) and $\mathbf{f}$ the body force per unit volume (which in this case is set to zero). For a newtonian fluid the extra-stress tensor $\mathbf{T}$ is connected with the strain rate tensor $\mathbf{D} = \frac{1}{2}\left(\mathbf{L} + \mathbf{L}^{\mathbf{T}}\right)$ by $\mathbf{T} = 2\mu\mathbf{D}$, where μ is the fluid viscosity.

The simulation uses a standard Galerkin finite element method based on the isoparametric triangular Taylor-Hood element with continuous piecewise quadratic shape functions for the velocity and continuous piecewise linear ones for the pressure. The unstructured mesh used to discretize both the entrance and the mid-plane area of figure 2 is shown in figure 4. It describes the area $-2 \leq \xi \leq 22$ and $0 \leq \Psi \leq 4.1$. A close-up of the cylinder section can be seen in figure 10.

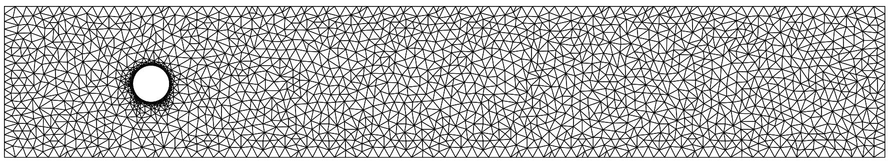

Fig. 4. Finite element mesh with ca. 17000 unknowns (u,v,p)

The above equations are supplemented with initial and boundary conditions all selected in such a way, that the resulting simulation will follow the experimental set-up as close as possible. Therefore the initial condition is a fluid at rest with zero velocities and zero pressure gradient. A no-slip boundary condition is used for all walls. It is assumed the time-varying inlet velocity can be approximated by

$$\mathbf{v}_{in}(y,t) = \mathbf{v}_s(y)\ \ f_p(t) \tag{5}$$

where index s refers to the stationary velocity of figure 3 as measured with the LDV equipment. The process function $f_p(t)$ describes the change in inlet velocity from 0 to $\mathbf{v}_s$ and is in this case assumed to be linear. It thus roughly approximates the quasi-linear curve in figure 9 as seen with LDV at $\xi = -2, \Psi = 2$. Different functions $f_p(t)$ will result in a different fluid structure only during the start-up, but not after the vortex shedding has started and the inlet velocity remains unchanged. The outflow condition is somewhat more complicated since no velocity data is available and the flow itself is, due to the vortex shedding, suspected to be very complex. A useful condition is to enforce a vanishing vertical velocity in combination with a vanishing horizontal tension vector, viz. $\mathbf{v} \times \mathbf{n} = 0$ and $\mathbf{t} \cdot \mathbf{n} = \mathbf{0}$ where $\mathbf{n}$ is the surface normal vector and $\mathbf{t} = -p\,\mathbf{n} + \mathbf{T} \cdot \mathbf{n}$ the tension vector. As shown in figure 6 this condition has no visible influence in upstream direction.

The spatial discretization leads to a semi-discrete coupled system of nonlinear differential ordinary equations. Applying an implicit time discretization (e.g.

Crank-Nicholson, second order in time) this results in an algebraic nonlinear indefinite system

$$\begin{pmatrix} \mathbf{N}(\mathbf{v}) & \mathbf{C} \\ \mathbf{C}^{\mathbf{T}} & \mathbf{0} \end{pmatrix} \begin{pmatrix} \mathbf{v} \\ \mathbf{p} \end{pmatrix} = \begin{pmatrix} \mathbf{n} \\ \mathbf{c} \end{pmatrix} \tag{6}$$

which then has to be solved at all timelevels. Formally solving the first equation for **v** and inserting the result in the second equation gives two definite nonlinear problems,

$$\mathbf{S}\,\mathbf{p} \;=\; \mathbf{C}^{\mathbf{T}}\,\mathbf{N}^{-1}\,\mathbf{C}\,\mathbf{p} = \mathbf{C}^{\mathbf{T}}\mathbf{N}^{-1}\,\mathbf{n} - \mathbf{c} \tag{7}$$

$$\mathbf{N}\,\mathbf{v} = \mathbf{n} - \mathbf{C}\,\mathbf{p}\;\;, \tag{8}$$

with the matrix **S** however given implicitly only. The solution algorithm solves the first equation using a variant of the well known Richardson-iteration, involving a suitable preconditioner for **S**. After the solution for **p** is known, the second equation can be solved for **v**. In practice, both equations are solved in a successive manner within the iteration process. A detailed description of the algorithm is given in [2].

The timestep size Δt is automatically selected using a local error estimation based on two similar integrations of different timesteps (one step with Δt, two steps with $\Delta t/2$) . At the begin a strong increase in the timestep length is seen in figure 5. It is interesting to note that later, with the vortex street fully developed, still a periodic change of then small steps is used.

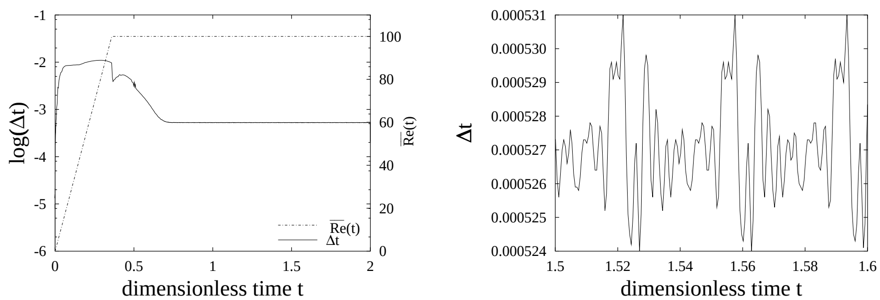

Fig. 5. Adaptive selection of the simulation timestep

The amount of computational time required for $0 \leq t \leq 2$ is ca. 28 h on a Sun Ultra 1 workstation using a workspace of ca. 12 MB. As an example for the flow computed by the simulation, figure 6 shows several streaklines during vortex shedding. The greyscales refer to different positions where tracer particles of zero mass have been added into the flow. Figure 7 gives a closer view of the quasi-stationary flow around the cylinder.

Besides the calculation of the velocity and pressure field, the simulation is also able to predict not easily measurable data, like drag and lift forces on the (two-dimensional) cylinder as a function of time. Figure 8 shows the corresponding dimensionless coefficients, which are defined as usual, viz. $C_D = F_D/(\rho/2u_m^2 D)$.

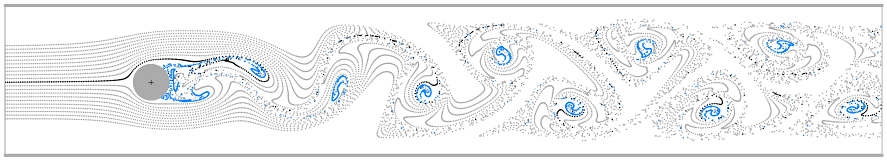

Fig. 6. Streaklines during vortex shedding

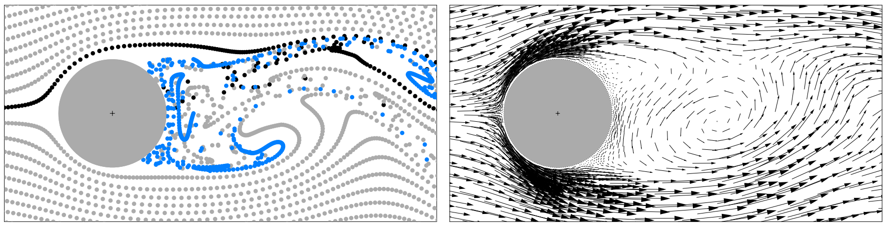

(a) Streaklines (b) Velocity Vectors

Fig. 7. Quasi-stationary streaklines and velocity vectors

Using such integral data the program code had previously been verified by computing the so called benchmark-flow described in [3] within the geometry of figure 2. As shown in [2], a very good agreement has been found. In fact, the investigation described here was inspired by that problem, since integral data alone, even if sensitive like the lift coefficient, is not sufficient for a complete validation of a simulation. In view of this there is a need for time-varying field information ($\mathbf{v}$, p) for other than pure academic problems. We hope the data presented here will help to somewhat narrow this gap.

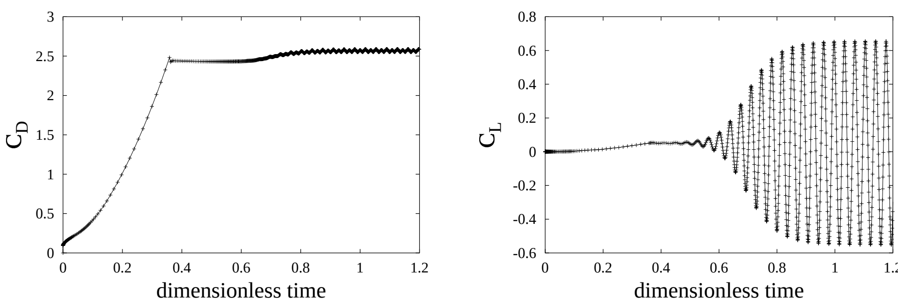

Fig. 8. Drag and lift coefficient C_D and C_L

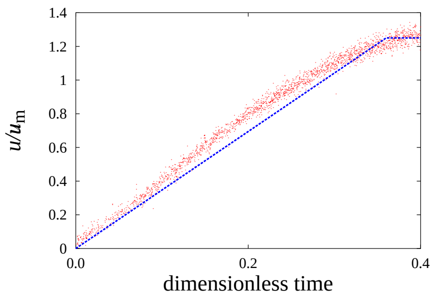

Fig. 9. Start-up of the inflow at $\xi = -2, \psi = 2$

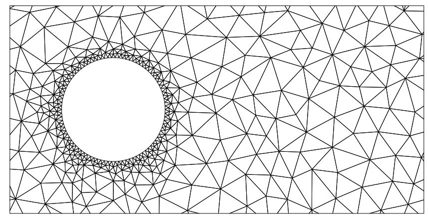

Fig. 10. Finite element mesh near cylinder

4 Results

4.1 Instationary Flow

We start the flow by opening the valve shown in figure 1. The mean velocity of the flow entering the investigation area increases nearly linearly from zero to its maximum value during a time intervall of $\Delta\tilde{t} = 0.35$. It is measured at $(\xi = -2, \psi = 2)$ with LDV (see figure 9, points: LDV-data, line: approximation for simulation). Afterwards the mass flow is kept constant and then we measure the inflow velocity profile at $(\xi = -2, \psi)$ with LDV (see figure 3). As described previously, both data sets are used for the simulation.

In figure 11 we show the velocity at point 4 as measured by LDV. The velocity increases during start-up and shows oscillations immediateley after the mass flow is constant. Comparing this curve to the corresponding simulation data, we find very good agreement for both the amplitude and the frequency. The earlier start of the oscillations in the experiment may be caused by small disturbances in the set-up.

Results of PIV-measurements during start-up are shown in figure 12. As examples for instationary and non-periodic flow fields streamlines and vorticity (left) and velocity vectors (right) are shown for two different moments when vortex shedding has not yet started. One can observe an increasing area of slack water where the velocities are close to zero. The vorticity intrudes into the flow from the cylinder and the channel walls and increases in magnitude as it is indicated by the darker gray of the contour plot.

4.2 Quasistationary Flow

When constant mass flow is reached, we measure the velocity with LDV at points 1–11 and take images for PIV within the rectangle shown in figure 2. With LDV as a point measurement technique we are not able to capture the velocities at different points at the same instant as it can be done with the simulation or with PIV. Therefore we choose an arbitrary time interval of $\Delta\tilde{t} = 0.2$ and compare LDV and PIV data to the simulation data, keeping in mind that the phase of the velocity oscillations will be different. Further on, for LDV the shape (the temporal resolution) of the curves strongly depends on the number of particles passing the measuring volume, whereas for PIV and the simulation the shape of the curves strongly depends on the image capturing freqency respectively the simulation timestep. In these experiments PIV image pairs are taken with a frequency of 1.3 Hz, which is sufficient to capture the main flow structures caused by the shedding of the vortices (according to the NYQUIST criterion). The frequency can be increased up to 15 Hz so that even faster oscillations can be observed with PIV.

In the following results of PIV, LDV and simulation for two measuring points (3 and 4) are reviewed. In general, experiments and numerical simulation agree well with respect to both qualitative and quantitative behaviour. The shape of the oscillations are given likewise with all methods (see figures 13 – 18). Even striking fine structures of the vertical velocity are found in both experiments and simulation (see figures 13(b), 14(b) and 15(b)). The marks in the figures represent measured particles (LDV), results of cross-correlating successive image pairs (PIV) and timesteps (simulation). The different amplitudes of the horizontal velocity may be caused by an uncertainty with which the actual location of the measuring points can be accessed in the experiment. The Strouhal number derived from the measurements is between 0.271 (PIV) and 0.281 (LDV) and computed to be 0.283 in the simulation.

Further on, PIV is used to gain experimental data of the time dependent velocities within a plane orientated normally to the cylinder axis. It is not possible to get similar velocity maps of flows like the instationary vortex street with LDV because as a point measurement technique LDV can only be used to record velocities at a single point over time. Figures 19 and 20 show the contour plot of the absolute velocity and streamlines of the flow. To reduce the amount of presented data only every second PIV image pair ($\Delta\tilde{t} = 6 \cdot 10^{-3}$) and the corresponding result of the simulation are shown. The unusual means of streamlines for instationary flows is chosen in order to visualize the positions of the vortices. The 20 grayscales for the dimensionless absolute velocity represent a value of 0 with white and a value of 2.0 with dark gray. One can find very good agreement in the position of the vortices and the form of the streamlines.

Figures 21 and 22 show a detailed view around measuring point 1 for the same points in time as in figures 19 and 20. One can observe a vortex core moving from the upper left corner down to the lower right corner. Again very good agreement between experiment and simulation is shown.

5 Conclusions

The PIV and LDV measurements make experimental information on the time dependent development of the velocities in the *Kármán vortex street* available for a whole cross-section and at discrete points for comparison with numerical simulations. In spite of the actual three dimensionality and the wall influences[2] excellent agreement between experiments and two dimensional simulation can be found.

The results of the PIV measurements prove that it is possible to extend the application of PIV away from statistical evaluation of turbulent flows towards to the recording of instationary flows that cannot be triggered to external events—like it is possible in turbo machinery—and therefore cannot be recorded by LDV.

References

[1] EISENLOHR, HOLGER und HELMUT ECKELMANN. *Vortex splitting and its consequences in the vortex street wake of cylinders at low Reynolds number*. Physics of Fluids A, **1** (2): (1990) 189–192.

[2] LUND, CHRISTOPH. *Ein Verfahren zur numerischen Simulation instationärer Strömungen mit nichtlinear-viskosen Fließeigenschaften*. VDI-Verlag GmbH, Düsseldorf, 1998.

[3] TUREK, S. und M. SCHÄFER. *Benchmark computations of laminar flow around cylinder*. In E. H. Hirschel (Hg.), *Flow Simulation with High-Performance Computers II*, Bd. 52 von *Notes on Numerical Fluid Mechanics*. Vieweg, 1996: S. 547–566. (support of F. Durst, E. Krause, R. Rannacher).

[4] WILLIAMSON, C. H. K. *Oblique and parallel modes of vortex shedding in the wake of a circular cylinder at low Reynolds numbers*. Journal of Fluid Mechanics, **206**: (1989) 579–627.

[2]See [4] and [1] for the sensitiveness of the *Kármán vortex street* against three dimensional effects.

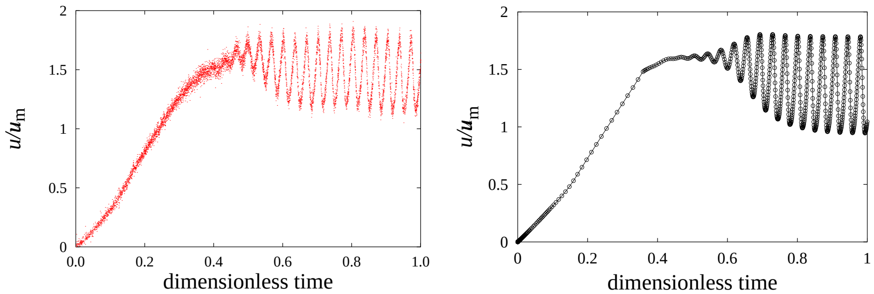

(a) Results of LDV (b) Results of simulation

Fig. 11. Horizontal velocity at point 4 during start-up

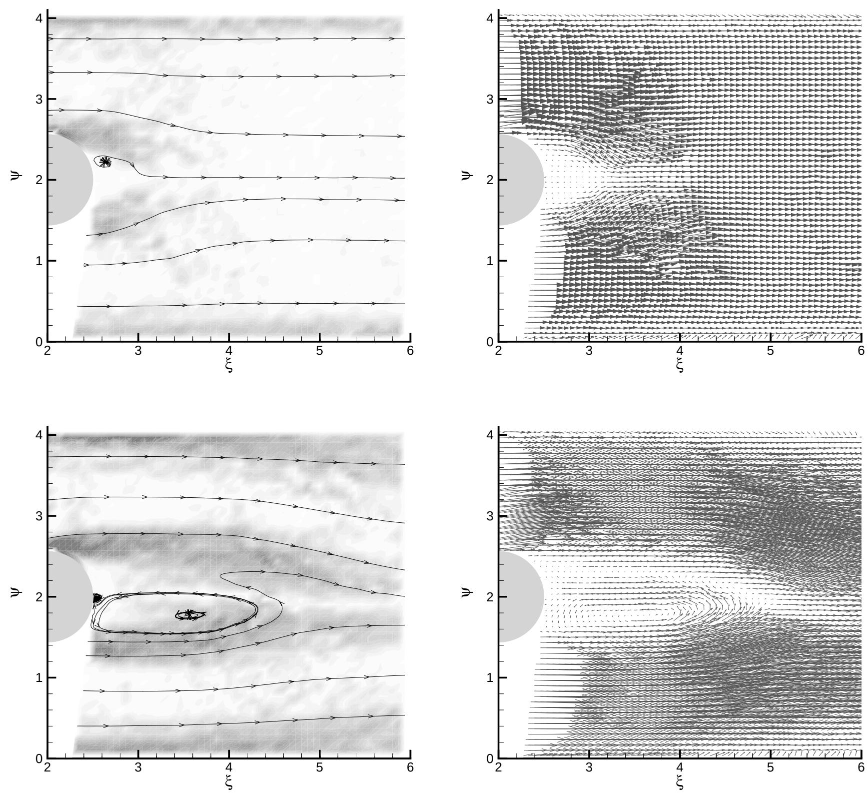

Fig. 12. PIV results during start-up (top: $\tilde{t} = 0.144$, right: $\tilde{t} = 0.324$); streamlines and vorticity (left), velocity vectors (right)

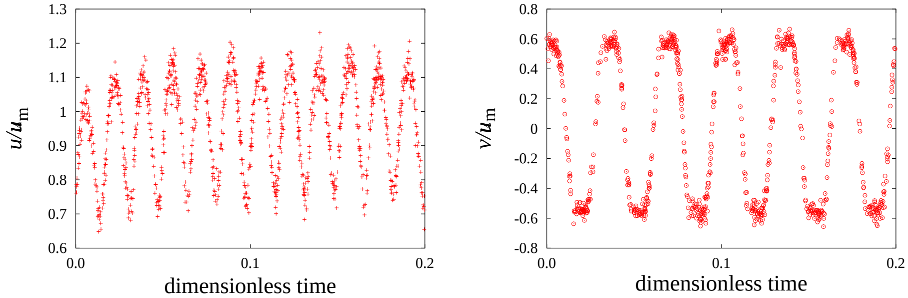

(a) Horizontal velocity

(b) Vertical velocity

Fig. 13. Results of LDV at point 3

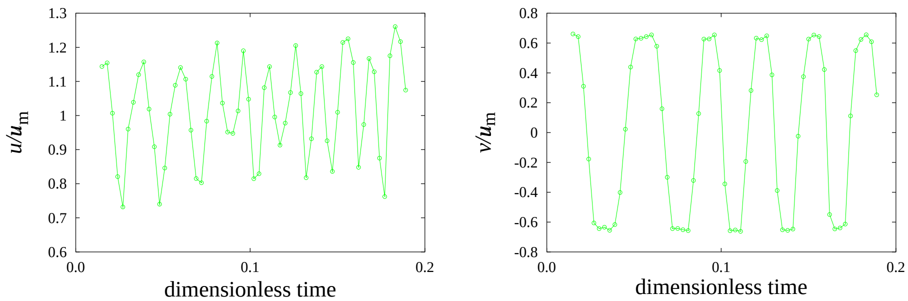

(a) Horizontal velocity

(b) Vertical velocity

Fig. 14. Results of PIV at point 3

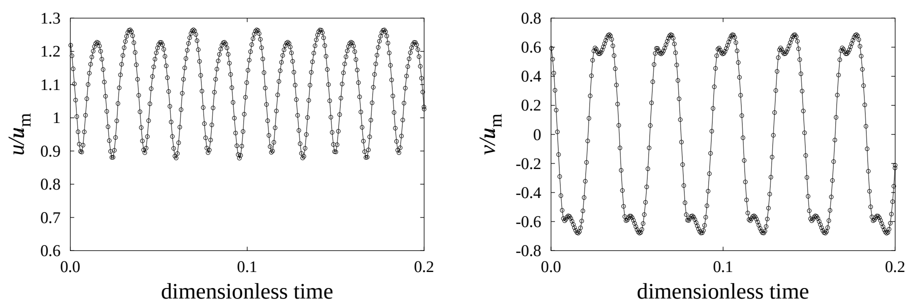

(a) Horizontal velocity

(b) Vertical velocity

Fig. 15. Results of simulation at point 3

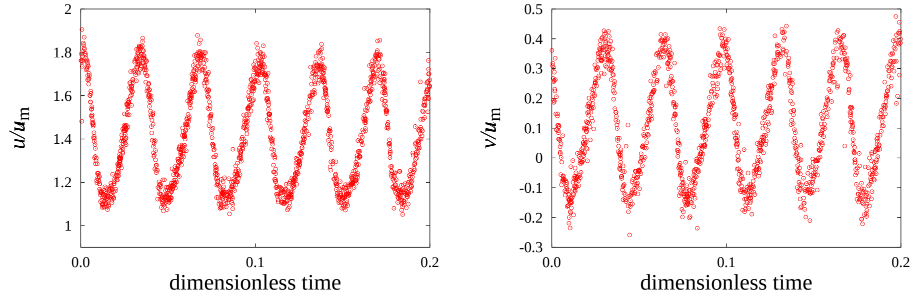

(a) Horizontal velocity (b) Vertical velocity

Fig. 16. Results of LDV at point 4

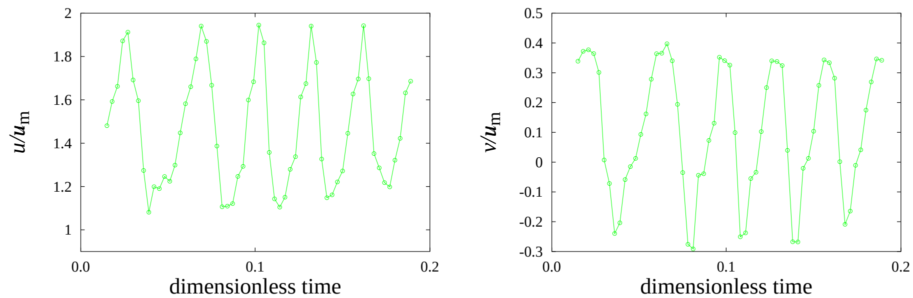

(a) Horizontal velocity (b) Vertical velocity

Fig. 17. Results of PIV at point 4

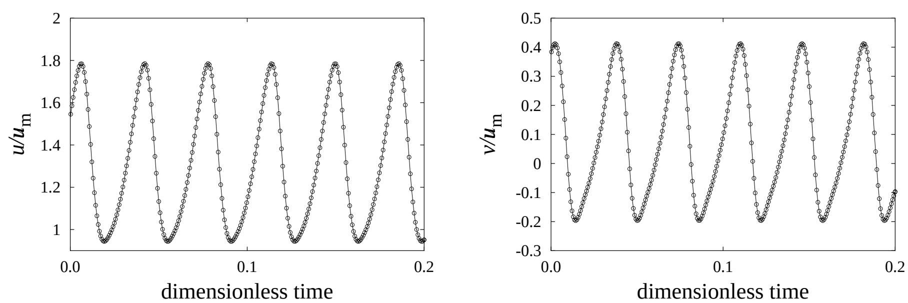

(a) Horizontal velocity (b) Vertical velocity

Fig. 18. Results of simulation at point 4

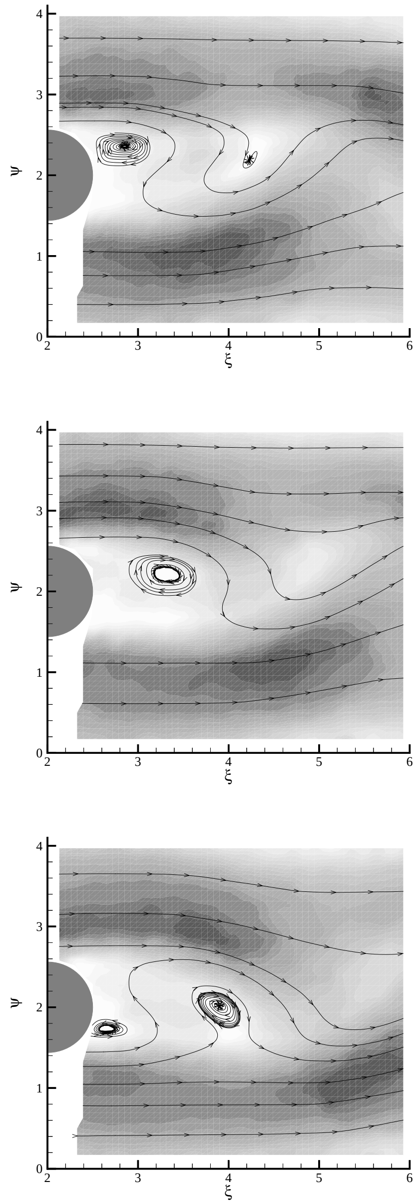

Fig. 19. Contour plot of absolute velocity and streamlines—PIV

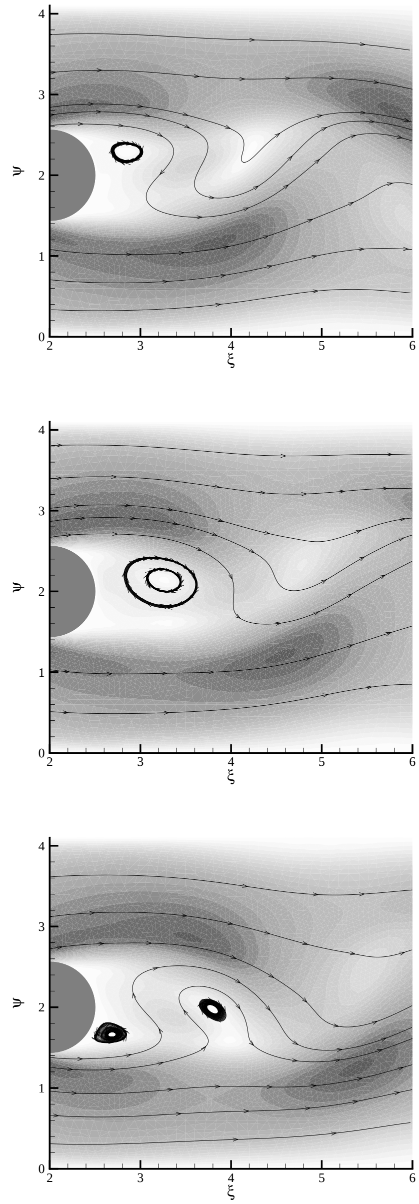

Fig. 20. Contour plot of absolute velocity and streamlines—simulation

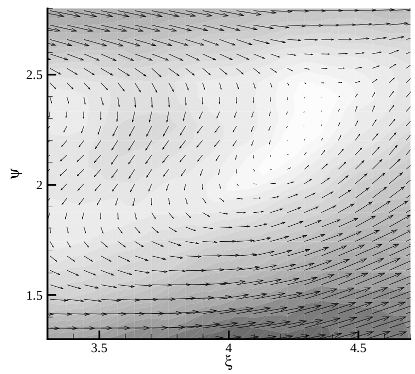

Fig. 21. Contour plot of absolute velocity and velocity vectors—PIV

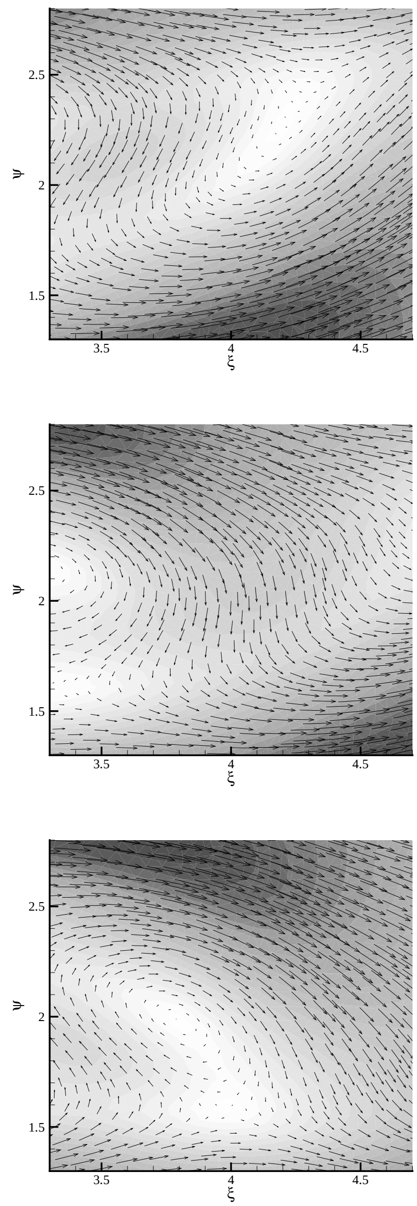

Fig. 22. Contour plot of absolute velocity and velocity vectors—simulation